Composites Part B 177 (2019) 107438

Contents lists available at ScienceDirect

Composites Part B

journal homepage: www.elsevier.com/locate/compositesb

Self-constructed nanodomain structure in thermosetting blend based on the dynamic reactions of cyanate ester and epoxy resins and its related property

Song Chen, Li Yuan *, Zehao Wang, Aijuan Gu, Guozheng Liang

Jiangsu Key Laboratory of Advanced Functional Polymer Design and Application, Department of Polymer Science and Engineering, College of Chemistry, Chemical Engineering and Materials Science, Soochow University, Suzhou, 215123, PR China

ARTICLE INFO

Keywords:
Nano structures
Smart materials
Thermosetting resin
Mechanical properties
Thermal properties

ABSTRACT

A new strategy to obtain nanodomain structure in thermoset/thermoset blends was developed via different dynamic reactions of cyanate ester (CE) and epoxy (EP) resins in the presence of zinc (II) acetylacetonate and glutaric anhydride. The resulting polymer systems show high mechanical property mainly attributed to EP nanophase and the excellent interfacial interaction between EP nanophase and CE matrix. Owing to the broad glass transition, the polymer systems display thermally activated triple shape memory effects in the temperature ranges of 150–225 °C. Moreover, the systems exhibit thermal self-healing behavior resulting from the trans-esterification and possible reactions between the residual cyanate ester and epoxy groups, and a 78–83% recovery of fracture toughness for the resulting polymers can be achieved after the first healing schedule of 200 °C/2 h.

1. Introduction

Thermosetting polymers with nano structures have been developed rapidly in the past decade and received great interest by researchers due to their unique properties that are often rather different from those of conventional materials in mechanics, optics, magnetism, therotics electricity and so on [1–5]. In situ formation of nanostructure in polymer blend is a promising method, with this method, the present key problem on poor dispersion of nanopahse is solved aptly. Generally, two strategies have been proposed to develop in situ nanostructure within thermosetting polymer matrix.

The first is incorporating thermoplastic into thermosetting resins to form thermoplastic nanophase separated structure in thermosetting polymer matrix [6]. Because thermoplastics and thermosetting resins form a highly immiscibility blend, polymerization-induced phase separation is often used to obtain two-phase polymers [7]. For example, polyether sulfone, end-chain modified polyether sulfone, polysulfone and poly(ε-caprolactone), a liquid carboxylterminated acrlonitrile-butadiene rubber are introduced into thermosetting resins to obtain nanophase separated structures [8–10]. However, the immiscible thermoplastic/-thermosetting systems have a coarse morphology and poor adhesion between the two components.

The second is introducing block copolymers into thermosetting for creating nanostructures within thermosetting polymer matrix [11–13]. Owing to the improved compatibility of the blended components, block copolymer can be limited the scale of phase separation, thus the nanoscale microstructure in the thermosetting polymer can be created easily [12,13]. For instance, epoxidized styrene-block-butadiene-block-styrene triblock copolymer is added to epoxy (EP) resin to obtain spherical nanoparticles with diamater of 20–30 nm in EP matrix [14]. Low-molecular-weight poly (ethylene oxide)-poly(ethylene-alt-propylene) and poly(ε-caprolactone)--block-poly(dimethyl siloxane)-block-poly(ε-caprolactone) triblock copolymer are introduced to EP resins to fabricate nanostructured thermosets, and various nanostructures such as lamellar, cubic bicontinuous, hexagonally packed cylinders, etc. can be formed depending on the concentration of EP resins [15,16]. Polystyrene-block-polybutadieneblock-poly (methyl methacrylate) ABC triblock copolymers and poly(ethylene oxide)-block-polyethylene diblock can accelerate the formation of nanostructures in thermosetting resins [17,18]. Owing to the formation of nanostructures, the polymer blends can be considered as macroscopically homogeneous materials. However, it can be noticed that for easily constructing nanophase structures, at least one end of the polymer chain must be incompatible with thermosetting resin to ensure phase separation [15–19], then the adhesion between the two components is relatively weak. Guo and coworkers have reported that the introduction of block ionomer sulfonated polystyrene-block-poly(ethylene-cobutylene)-block-polystyrene (SSEBS) or their complexes in EP resin can successfully self-organize nano-scaled phase structure [20,21], and the sulfonic acid

* Corresponding author.
E-mail address: yuanli@suda.edu.cn (L. Yuan).

https://doi.org/10.1016/j.compositesb.2019.107438
Received 14 April 2019; Received in revised form 18 July 2019; Accepted 10 September 2019
Available online 11 September 2019
1359-8368/

groups or a tertiary amine-terminated poly(ε-caprolactone) blocks in the block ionomer complex can form hydrogen bonding with EP that significantly improves the adhesion between the components. It is great significance to improve the adhesion between nanostructure phase and polymer matrix for the outstanding mechanical property.

As we know, most thermoset/thermoset blends can form compatible formulation blends and the strong chemical or physical interactions between the different components can be realized because of their copolymerization or the formation of interpenetrating polymer networks [22,23]. Then, the excellent adhesion between thermosetting nanophase and thermosetting matrix can be easily obtained if the nanophase structure can be formed in situ in compatible thermoset/thermoset blends under reasonable condtions, and the resulting polymers may show some unexpected properties. Actually, it is hard to achieve phase-separated structure for thermoset/thermoset blends because of the lower Flory-Huggins interaction parameter in polymer blends and similar molecular weight of the blends [24]. Generally, the compatible formulation blends can easily form copolymer and interpenetrating polymer that have structured at molecular scales [25], thermoplastics and block copolymers are used to form nano-scaled phase structure in epoxy mainly owing to the partially compatible, and the macro-scaled phase structures are usually generated by conventional toughened because they are highly incompatible blends [25,26]. But for fully compatible blends, researchers believe that phase-separated structure can be induced in a narrow channel of composition. Few examples of such blends are benzoxazine/cyanate ester (CE) and benzoxazine/bismaleimide blend, in which sea-island phase structure and bi-continuous phase separated morphology can be formed by controlling reaction [27]. Since the strong interfacial adhesion between the separed-phase and matrix can be easily achieved in compatible blends, some unexpected properties may be obtained.

CE resins are representative high performance thermosetting resins and the cured CE resins are gifted with attractive properties such as excellent thermal property and high glass transition temperature. However, the inherent brittleness of the cured CE resins has limited its development and application owing to the rigid triazine networks. Then the toughness of the cured CE needs improvement. As compared with CE, EP resins display lower thermal property but better toughness and processing. In commercial applications, CE resins are often modified with EP to form compatible formulation blends with improved processibility and toughness [28]. In addition, microcracks are always generated within brittle thermosetting matrix, and previous studies have indicated that dynamic covalent bonds such as dynamic transesterification bonds can render polymers good healing ability at 150–230 °C without changing the crosslinking density [29–31]. For EP resins, the β-hydroxy ester bonds can be easily introduced into EP polymers through the reaction of hydroxyl/epoxy groups in EP and glutaric anhydride (GA) in the presence of zinc (II) acetylacetonate (ZAA), and the transesterification reaction between ester groups and β-hydroxyl groups can also happen in the presence of ZAA under controlled conditions, which can heal the microcracks within polymer matrix and recover the properties of polymers [29,32–34]. So, ZAA and GA are encouraged to appear in the EP systems. Furthermore, it is interesting to note that the polymerization of both CE and EP can be initiated by the same curing agents or catalyst such as amine derivatives and organometallic compounds at different temperature procedures [28,35], then it is a great opportunity to create phase-separated morphology by controlling reaction. As mentioned above, CE resins are often modified with EP for the better processability and improved toughness, then the nanodomains of EP polymers in CE matrix are expected for improving the property and developing new features of CE.

In this work, to improve and extend the properties of thermosetting CE/EP blends, in situ nanodomain structure in miscible thermosetting CE/EP blends is self-constructed in the presence of catalyst of zinc (II) acetylacetonate (ZAA) and glutaric anhydride (GA) and the interface interaction between two phases can be consolidated through the reaction of CE and EP. The morphologies of the nanodomain structure are probed, and the mechanical property and thermal property of the resulting systems are investigated. Also, the resulting polymer systems are supposed to possess the shape memory behavior and self-healing ability because of their broad glass transition temperature and the dynamic reversible covalent bonds inside the polymer systems [36,37]. In our previous work [29], although thermosetting EP and chain-extended bismaleimide (CBMI) were blended to obtain thermosetting systems with high thermal stability and dual memory effect, and GA and ZAA were introduced to the systems for designing dynamic transesterification bonds to heal or reconfigure the polymer systems, EP could easily react with CBMI at about 140 °C owing to the amino functional groups in CBMI as well as with GA in the presence of ZAA. Then the resulting EP/CBMI systems were cross-linked polymer networks based on EP/CBMI copolymers, which were significantly different from the thermosetting CE/EP blends with nanodomain structure presented in this paper. The aim of this paper is to present a novel strategy for designing in-situ nanostructured thermoset/thermoset blends with excellent mechanical property and other unexpected properties.

2. Experimental section

2.1. Materials

Diglycidyl ether of bisphenol A epoxy resin (EP, epoxy equivalent weight: 184–195 g/mol) was purchased from Nantong Xingchen Synthetic Materials Co., Ltd. (China). Cyanate ester [bisphenol A dicyanate (*2,2′*-bis(*4*-cyanatophenyl)isopropylidene, CE] was provided by Yangzhou Tianqi Material Co., Ltd. (China). Glutaric anhydride (GA) and zinc (II) acetylacetonate (ZAA) were purchased from Aladdin Industrial Corporation, China.

2.2. Preparation of CE/EP/GA/ZAA systems

A mixture of EP and GA was heated at 100 °C in glass breaker. When the solution became transparent, ZAA was added. The mixture was kept at 100 °C under stirring for 10 min, adding CE. After stirring at 100 °C for 20 min, the mixture was poured into a glass mold and placed in vacuum at 100 °C for releasing gases, subsequently was cured via the temperature procedure of 100 °C/1 h + 120 °C/6 h + 180 °C/1 h. In this work, polymers with three formulations were prepared, and the weight ratios of CE/EP/GA/ZAA were 60/40/12/4, 50/50/15/5 and 40/60/18/6, respectively, the corresponding polymer systems were coded as 60CE/40 EP/GA/ZAA, 50CE/50 EP/GA/ZAA and 40CE/60 EP/GA/ZAA, respectively. The ratio between EP and GA was calculated according to the stoichiometric ratio of epoxy group to anhydride [31], and the weight ratio of EP/GA/ZAA in all CE/EP/ZA/GAA systems was fixed at 10/3/1. ZAA was used as a promoter to accelerate the reaction of EP/ZAA as well as the reaction of CE. But for CE, very low concentration of ZAA could quickly catalyze the polymerization of CE [28], then it could be neglected as compared to the concentration of ZAA for catalyzing the reaction of EP/GA. It must be mentioned that during the preparing process of CE/EP/ZA/GAA systems, ZAA was mixed with EP/GA at 100 °C for 10 min before adding CE, then the concentration of ZAA was more highly diluted. Although the ratio of CE to ZAA with the content of EP/GA/ZAA varied, the ratio of CE to ZAA changed slightly. Because CE/EP blends are thermodynamically stable system [28], to form a uniformly dispersed phase structure in CE/EP blends, the co-continuous blends were encouraged [38]. Therefore, the weight ratios of CE to EP were expected to have smaller difference. However, CE/EP systems with larger ratios such as 10/90 or 90/10 were prepared for differentiating the samples (60CE/40 EP/GA/ZAA, 50CE/50 EP/GA/ZAA and 40CE/60 EP/GA/ZAA). For comparison, samples EP/GA/ZAA (10/3/1) and CE/ZAA were prepared using the similar temperature procedure to CE/EP/ZA/GAA systems, and EP/GA (10/3) and CE were prepared using higher cure temperature procedure of 100

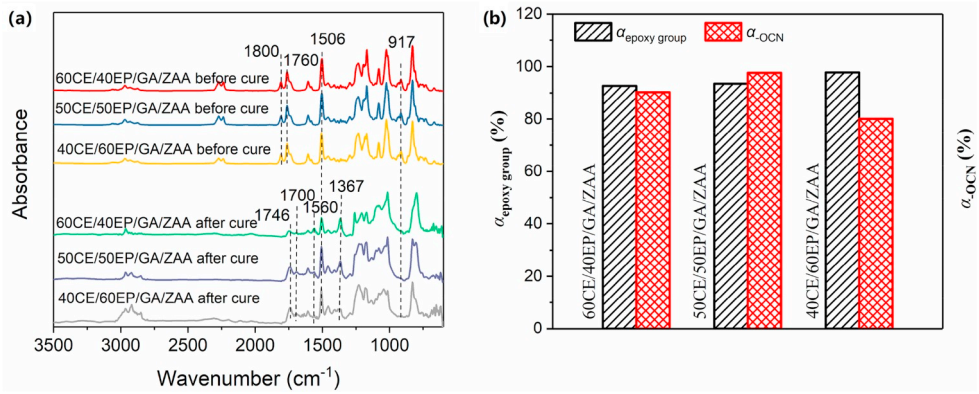

Fig. 1. FTIR spectra of CE/EP/GA/ZAA systems (a) and $\alpha_{\text{epoxy group}}$ and $\alpha_{\text{-OCN}}$ (b).

°C/1 h + 120 °C/6 h + 180 °C/2 h + 200 °C/2 h + 220 °C/2 h for considering their lower reaction rate (Fig. S1) [28]. It is hard to prepare CE/ZAA with the same ZAA content in CE/EP/GA/ZAA system owing to the very rapid catalytic polymerization of CE, only very lower concentration of ZAA was added for successfully preparing CE/ZAA, here the concentration of ZAA in CE/ZAA relative to CE was 0.05 wt%. EP was hard to self-polymerize to form crosslinked polymers that couldn't be used as reference as indicated by the DSC curve of EP (Fig. S1). The possible main reactions during the preparation of CE/EP/ZA/GAA systems are presented in Scheme S1 [28].

2.3. Characterization

Attenuated total reflection Fourier transform infrared (ATR-FTIR) spectra were obtained using a Bruker Vertex 70 spectrometer (Germany). The conversion of epoxy groups ($\alpha_{\text{epoxy group}}$) and cyanate groups ($\alpha_{\text{-OCN}}$) were estimated using internal standard method, and the peak of aromatic ring at 1506 cm^{-1} was selected as reference.

The morphologies of samples were observed using a scanning electron microscope (SEM, Hitachi S-4700, Japan), light microscope (VHX 5000) and digital camera.

Thermal properties were investigated using thermogravimetric analyzer (TGA, TA Discovery TGA Instrument) and differential scanning calorimetry (DSC, Q200 TA Instrument) at a heating rate of 10 °C/min under nitrogen atmosphere.

Dynamic mechanical analysis (DMA) of sample was tested on a TA Instrument DMA Q800 at frequency of 1 Hz and a heating rate of 3 °C/min. The dimensions of samples were 35 mm × 12 mm × 3 mm. The glass transition temperature (T_g) was defined by the peak temperature of *tanδ* curve. The crosslinking density (X_{density}) was evaluated based on the storage modulus at temperature T ($T = T_g + 50$ °C) according to Eq. (1).

$$\log_{10}G' = 7 + 293X_{\text{density}} \quad (1)$$

Atomic force microscopy (AFM) was utilized to characterize surface topography using Bruker Dimension Icon AFM (Germany). A peakfore tapping mode was employed to analyze the modulus with an aluminum reflex-coated silicon cantilever probe under the resonance frequency of 75 kHz. The nominal force constant was 3 N m^{-1}.

Transmission electron microscopy (TEM) was attained using a FEI Tecnai G-20 TEM at 200 kV. An ultra-microtome was used to obtain ultrathin sections.

The triple-shape memory behaviors were evaluated using DMA instrument under a tensile force-controlled mode. The rectangular samples were heated to a higher temperature T_{trans1} (T_g increased by about 30 °C) and then stretched to a temporary shape (S1) from its original shape (S0), writing down the strain under load ($\varepsilon_{s1,load}$). The deformed sample was cooled to lower temperature T_{trans2} (T_g reduced by about 20 °C) and unloaded the force, writing down the strain under unloading (ε_{s1}). Subsequently, the sample was continued to be deformed to another temporary shape (S2) under external force, cooled to room temperature and unloaded the force, writing down the strain under load ($\varepsilon_{s2,load}$) and unloading (ε_{s2}). Reheating the deformed sample to T_{trans2} and T_{trans1}, respectively, temporary shapes S2 and S1 could recover to S1 and then to S0, writing down the corresponding strains after recovery ($\varepsilon_{s1,rec}$ and $\varepsilon_{s0,rec}$). The R_f and R_r were calculated according to the following Eqs. (2) and (3) [39].

$$R_f(x \to y) = \left(\frac{\varepsilon_y - \varepsilon_x}{\varepsilon_{y,load} - \varepsilon_x}\right) \times 100\% \quad (2)$$

$$R_r(x \to y) = \left(\frac{\varepsilon_x (or\ \varepsilon_{x,rec}) - \varepsilon_{y,rec}}{\varepsilon_x - \varepsilon_y}\right) \times 100\% \quad (3)$$

where x and y represented different shape (S2, S1 and S0).

Flexural strength was measured using an electronic universal testing machine (CMT-4104, China) according to GB/T 2567-2008 at a speed of 2 mm/min.

Fracture toughness (K_{IC}) was measured using standard single-edge notched beam (SENB) specimens. The length (L), width (W) and thickness (T) of samples were 38 mm, 7 mm and 3.5 mm, respectively. The notch was cut with a diamond saw, then generating a pre-crack by gently tapping a fresh razor blade at the base of the notch. The length (α) of pre-crack was controlled between 0.45W and 0.7W. The samples were tested using the electronic universal testing machine at a constant displacement rate of 0.5 mm/min. Fractured specimens were healed at 200 °C for 2 h after the two crack surfaces were contacted each other tightly. After healing procedure, owing to the healing of the crack surfaces, the pre-cracks should be made again using the same method for generating pre-crack as mentioned above. The healing efficiency (η) was the ratio of the K_{IC} after healing ($K_{\text{IC healed}}$) to the original K_{IC} ($K_{\text{IC origin}}$). Fig. S2 shows the dimensions of SENB specimen.

3. Results and discussion

3.1. Structure and morphology of polymer systems

Changes of characteristic functional groups in CE/EP/GA/ZAA systems before and after cure can be investigated using FTIR as shown in Fig. 1. The FTIR spectra (Fig. 1a) of CE/EP/GA/ZAA systems before cure present the characteristic absorption peaks of epoxy groups, cyanate ester (−OCN) groups and C═C of aromatic ring at 917 cm^{-1}, 2274−2235 cm^{-1} and 1506 cm^{-1}, respectively, they also show the distinct characteristic absorption peaks of anhydrides at 1800 cm^{-1} and 1760 cm^{-1}. As compared to CE/EP/GA/ZAA systems before cure, the cured CE/EP/GA/ZAA systems have weak or disappeared absorption peaks of epoxy and –OCN groups as indicated by their FTIR spectra. However, some new absorption peaks appear at 1700 cm^{-1}, 1560 cm^{-1}

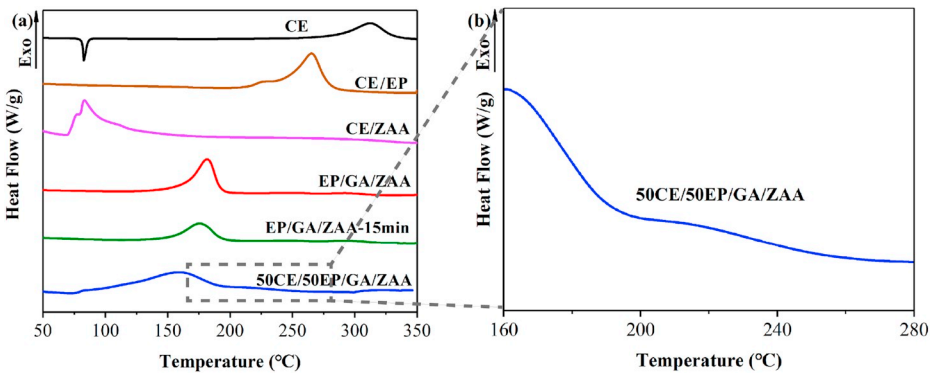

Fig. 2. DSC curves of CE, CE/EP, CE/ZAA, EP/GA/ZAA and CE/EP/GA/ZAA system.

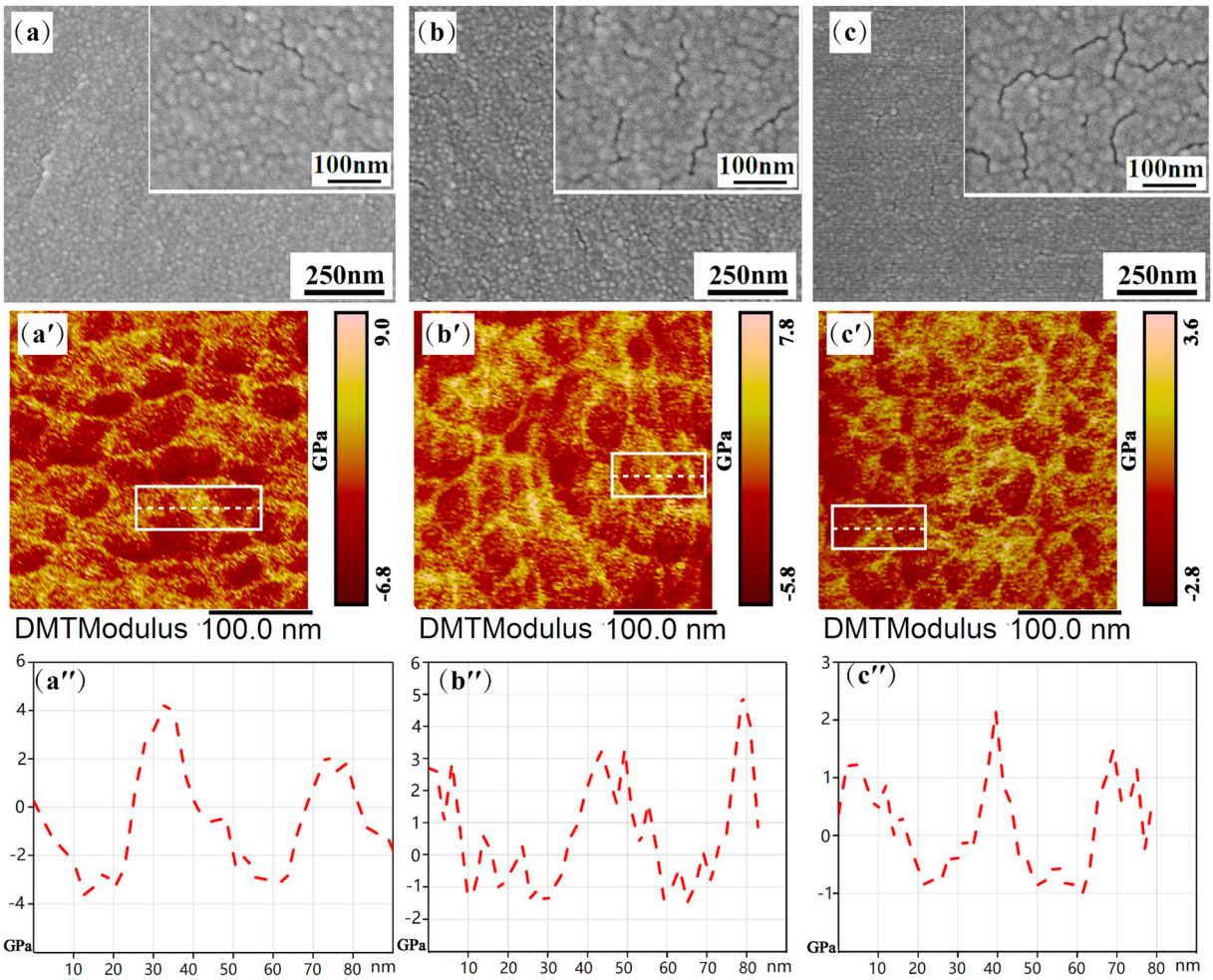

Fig. 3. SEM and AFM images of the fracture surfaces of the cured CE/EP/GA/ZAA systems and the curves of distance modulus of the representative cross sections marked by dashed lines: (a, a′ and a″) 60CE/40 EP/GA/ZAA, (b, b′ and b″) 50CE/50 EP/GA/ZAA and (c, c′ and c″) 40CE/60 EP/GA/ZAA.

and 1367 cm^{-1}, which are attributed to the stretching vibration characteristic absorption peaks of carbonyl group in ester and triazine ring, respectively, resulting from the reaction of epoxy with GA and the polymerization of CE in the presence of ZAA (Scheme S1). Additionally, an absorption peak at 1746 cm^{-1} can be observed in the FTIR curves of CE/EP/GA/ZAA systems, which is caused by the oxazoline groups formed by the reaction of –OCN and epoxy group.

For 60CE/40 EP/GA/ZAA, 50CE/50 EP/GA/ZAA and 40CE/60 EP/GA/ZAA systems, the calculated $\alpha_{\text{epoxy group}}$ values are 93%, 94% and 98%, respectively, which gradually increase with EP/GA/ZAA content (Fig. 1b), this phenomenon is attributed to the fact that the increased EP/GA/ZAA concentration can improve the polymer reaction rate of EP. The calculated $\alpha_{\text{-OCN}}$ values are 90%, 98% and 80% (Fig. 1b), respectively, which increases with EP/GA/ZAA content first and then decreases when the weight ratio of CE/EP is 40/60, the reason is the fact that the slightly higher ZAA concentration in polymer systems can lead to the faster polymerization of CE that limits the diffusion of CE monomer and results in the incomplete reaction of CE.

To further clarify the possible reactions of CE/EP/GA/ZAA system, DSC experiments were performed as shown in Fig. 2. For CE monomer,

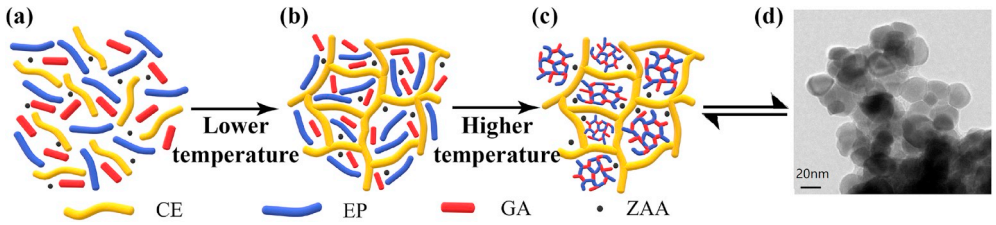

Fig. 4. Schematic of in situ formation mechanism (a–c) and TEM image of the nanostructure in 60CE/40 EP/GA/ZAA system (d).

the endothermic peak at 82 °C is caused by the melting point, and the exothermic peak at 312 °C is attributed to the self-polymerization of –OCN groups. Evidently, EP can accelerate the reaction of CE because the exothermic peak temperature of CE/EP is about 265 °C that is lower than that of CE. The reaction between CE and EP can explain the excellent compatibility between CE and EP. Furthermore, the addition of ZAA can quickly catalyze the reaction of CE, which can be indicated by the very low exothermic peak temperature (about 83 °C) of CE/ZAA. The EP/GA/ZAA shows an exothermic reaction peak at 181 °C. Because ZAA can significantly catalyze the reaction of CE, a weak peak at about 79 °C in the DSC curve of 50CE/50 EP/GA/ZAA system should be attributed to the catalytic reaction of CE and the significant exothermic peak at 160 °C must be caused by the reaction of EP/GA/ZAA, which demonstrate a two-stage curing for CE/EP/GA/ZAA system at lower temperature and the main reactions occurred in CE/EP/GA/ZAA systems is not copolymerization. However, a weak shoulder exothermic peak at about 220 °C in the DSC curve of 50CE/50 EP/GA/ZAA can indicate the reaction between CE and EP, demonstrating that the interface interaction between CE and EP phases can be improved at higher temperature.

To confirm the morphology of CE/EP/GA/ZAA system, SEM and AFM experiments were conducted. Fig. 3 shows the SEM and AFM images of the fracture surface of the cured CE/EP/GA/ZAA systems. The SEM images of the fracture surfaces of the cured 60CE/40 EP/GA/ZAA, 50CE/50 EP/GA/ZAA and 40CE/60 EP/GA/ZAA clearly demonstrate nanodomain structure (Fig. 3a—3c), which can prove the formation of two different crosslinked polymer networks. The discrete interlaced patterns (Fig. 3a—3c) are very different from the smooth and glassy surfaces of fractured CE, CE/ZAA, EP/GA and EP/GA/ZAA systems (Fig. S3).

The AFM images also show the nanodomain structure, the darker domain represents the lower modulus EP nanodomain, which can be indicated by the storage moduli of EP/GA (or EP/GA/ZAA) and CE (or CE/ZAA) polymers (Fig. S4a), whereas the bright area represents the higher modulus of CE polymers. The average sizes of the nanophase in 60CE/40 EP/GA/ZAA, 50CE/50 EP/GA/ZAA and 40CE/60 EP/GA/ZAA calculated from the curves of distance modulus (Fig. 3a″—3c″) are about 35 nm, 30 nm and 28 nm. It seems that lower content of CE can lead to smaller EP nanodomain, the most likely reason for this is the increased molecular diffusion of EP. Because CE and EP are compatible and CE can quickly react in the presence of ZAA to form the cross-linked networks that can restrict the molecular diffusion of EP, the decreased CE content can reduce the formation of the cross-linked networks, which is beneficial to the diffusion of EP molecules and the formation of slightly smaller EP nanodomain.

Fig. 4 shows a schematic of in situ formation mechanism of the nanodomain structure in CE/EP/GA/ZAA system and TEM image of the resulting CE/EP/GA/ZAA systems. During the heating process of CE/EP/GA/ZAA systems, CE has the priority to react in the presence of ZAA at lower temperature. With the increase of molecular weight and cross-linking degree of CE, EP micelles should be formed by reactive extrusion of CE [38,40]. But because CE resins and low molecular weight CE polymers are compatible with EP, and the strong electronic interaction between carbon atom of the –OCN in CE and oxygen atom of epoxy groups in EP can form due to their strongly electrophilic and nucleophilic behavior [28], the CE/EP blends should be thermodynamically stable systems at the nanometre scale during the early stage of the curing [38] (Fig. 2a). For CE/EP/GA/ZAA systems, ZAA can quickly induce the localized reactions of CE as indicated by the DSC curve of CE/ZAA, which can significantly decrease the molecular diffusion by several orders of magnitude during cure [28,41,42], then the EP molecules are hard to further gather together and the nanostructures of the EP domain can lock and well disperse in CE polymer systems (Fig. 4b). As the reaction time and temperature increase, the molecular weight of CE continues to increase, meanwhile EP starts to react as indicated by the DSC curves of EP/ZAA/GA and 50CE/50EP/ZAA/GA (Fig. 2a), Finally, EP nanodomains can be constructed in situ in blend systems (Fig. 4c). Since the formation of the EP domains is mainly controlled by the thermodynamic stability of the compatible resin systems before curing or during the early stage of the curing, which is related to the strong electronic interaction between carbon atom of the –OCN in CE and oxygen atom of epoxy groups, as well as controlled by the different dynamic reactions of CE and EP, the method for constructing EP nanodomain in CE/EP/GA/ZAA systems may be a combined technology based on self-assembly technology and reaction-induced phase separation, which is different from the traditional phase separation method that is based on the incompatibility of thermoplastic/thermosetting resins to fabricate nanostructure via reaction-induced phase separation

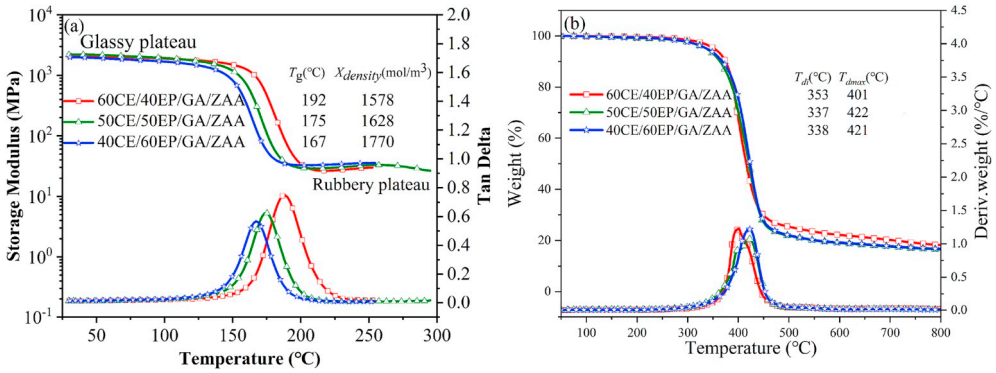

Fig. 5. DMA (a) and TGA (b) curves of CE/EP/GA/ZAA systems.

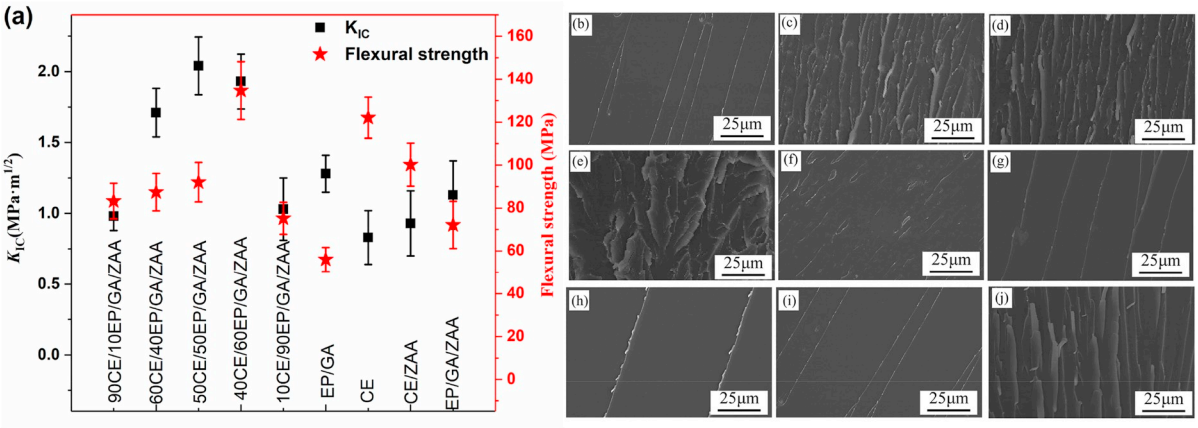

Fig. 6. Mechanical properties (a) of polymer systems and SEM images of fracture surfaces of 90CE/10 EP/GA/ZAA (b), 60CE/40 EP/GA/ZAA (c), 50CE/50 EP/GA/ZAA (d), 40CE/60 EP/GA/ZAA (e), 10CE/90 EP/GA/ZAA (f), EP/GA (g), CE (h), CE/AA (i) and EP/GA/ZAA (j).

mechanism [12]. Although CE can react with EP as implied by the DSC curve of CE/EP, high temperature is needed. It is remarkable that even when confined in self-constructed nanostructures, the copolymerization of CE and EP can happen as indicated by the DSC curves of CE/EP and 50CE/50EP/ZAA/GA. However, the reaction occurs only at the interface between the EP domain and CE matrix. The TEM image of CE/EP/-GA/ZAA system (Fig. 2b) can prove the existence of the nanodomain with about 30 nm in diameter. As compared to 60CE/40 EP/GA/ZAA, 50CE/50 EP/GA/ZAA and 40CE/60 EP/GA/ZAA, 90CE/10 EP/GA/ZAA and 10CE/90 EP/GA/ZAA have no obvious nanostructures (Fig. S3), the reason is the fact the lower concentration of CE or EP cannot induce obvious phase separation structure owing to the good compatibility of CE/EP. Leibler L and coworkers have reported that stable co-continuous polymer materials can structure at the nanometre scale by reactive blending [38]. Then when CE content is close to that of EP, co-continuous CE/EP/GA/ZAA systems can be easily formed and nanostructure can be constructed in CE/EP/GA/ZAA systems.

3.2. Dynamic mechanical property and thermal property

Fig. 5 shows the DMA and TGA curves of CE/EP/GA/ZAA systems. CE and CE/ZAA have higher storage moduli at glassy plateau and T_g values than EP/GA and EP/GA/ZAA mainly owing to the rigid triazine ring in CE polymers [28] (Fig. S4a). The storage moduli at glassy plateau of 60CE/40 EP/GA/ZAA, 50CE/50 EP/GA/ZAA and 40CE/60 EP/GA/-ZAA are about 2103 MPa, 2203 MPa and 1995 MPa that are between those of CE (or CE/ZAA) and EP/GA (or EP/GA/ZAA) (Fig. 5a) and when the temperature is over 200–250 °C they rapidly decrease to 30 MPa, 26 MPa and 35 MPa, respectively, corresponding to the storage moduli at rubbery plateau. The T_g values of 60CE/40 EP/GA/ZAA, 50CE/50 EP/GA/ZAA and 40CE/60 EP/GA/ZAA are 192 °C, 175 °C and 167 °C, which decrease with the increase of EP/GA/ZAA content, the reason is the increased soft segments resulting from the ring-opening reaction of epoxy group with glutaric anhydride and the reduced rigid triazine ring in the resulting polymers. However, the $X_{density}$ increases with the content of EP/GA/ZAA as listed in Fig. 5a, the reason is the fact that EP resins can effectively react with GA for their higher concentration in the system. To further understand the change tendency in storage moduli, T_g values and $X_{density}$ of CE/EP/GA/ZAA systems with EP/GA/ZAA content, 90CE/10 EP/GA/ZAA, 10CE/90 EP/GA/ZAA are prepared. It can be found that the storage moduli at glassy plateau, T_g and $X_{density}$ values of 60CE/40 EP/GA/ZAA, 50CE/50 EP/GA/ZAA and 40CE/60 EP/GA/ZAA are between those of 90CE/10 EP/GA/ZAA and 10CE/90 EP/GA/ZAA (Fig. S4a), the storage moduli and T_g generally decrease with EP/GA/ZAA, whereas $X_{density}$ increases. In this work, CE/EP/GA/ZAA systems have a single damping peaks, which suggests the excellent compatibility between CE and EP [43].

CE and CE/ZAA show much higher initial thermal decomposition temperatures at 5% weigh loss (T_{di}) and decomposition temperatures at the maximum weigh rate (T_{dmax}) than EP/GA and EP/GA/ZAA mainly owing to the rigid triazine ring and high aromatic ring content in CE polymers (Fig. S4b). All CE/EP/ZAA systems show lower T_{di} and T_{dmax} than CE and CE/ZAA possibly due to the decreased rigid triazine ring and aromatic ring. In this work, EP/GA and EP/GA/ZAA may show higher T_{di} or T_{dmax} than CE/EP/ZAA systems possibly owing to the increase of epoxy group conversion. The T_{di} values of 60CE/40 EP/GA/ZAA, 50CE/50 EP/GA/ZAA and 40CE/60 EP/GA/ZAA are 353 °C, 337 °C and 338 °C (Fig. 5b), which are much higher than the T_g of the corresponding samples, indicating that CE/EP/GA/ZAA systems are chemical thermal stability around T_g. The T_{di} of CE/EP/GA/ZAA may decrease with EP/GA/ZAA concentration first and then increase when the ratio of CE/EP is below 40/60, the reason for this is the combined effects of the decreased rigid triazine ring and aromatic ring and the increased $X_{density}$ and $\alpha_{\text{epoxy group}}$.

3.3. Mechanical properties

Fig. 6a shows the mechanical properties of 60CE/40 EP/GA/ZAA, 50CE/50 EP/GA/ZAA, 40CE/60 EP/GA/ZAA, EP/GA, CE, CE/ZAA and EP/GA/ZAA. CE and CE/ZAA have lower fracture toughness but higher flexural strength than EP/GA and EP/GA/ZAA mainly owing to the rigid triazine ring network. The fracture toughness (K_{IC}) and the flexural strength of 60CE/40 EP/GA/ZAA, 50CE/50 EP/GA/ZAA and 40CE/60 EP/GA/ZAA are 1.7–2.0 MPa $m^{1/2}$ and 87–135 MPa. Increasing EP/GA/ZAA content can improve the fracture toughness and flexural strength of CE/EP/GA/ZAA systems, the phenomena can be attributed to the increased soft segments resulting from reaction between epoxy resin and ZAA, and the increased $X_{density}$. More importantly, the formation of the nanophase structure can effectively toughen and reinforce the resulting polymers. From the SEM image (Fig. 3), the tortuous microcracks along the interface between nanodomain and CE matrix can be observed, which can prove that the presence of nanodomain can prolong crack propagation and increase the energy consumption. However, their fracture toughness cannot continue to increase when the weight ratio of CE/EP is beyond 50/50 possibly owing to the higher $X_{density}$. 60CE/40 EP/GA/ZAA, 50CE/50 EP/GA/ZAA and 40CE/60 EP/GA/ZAA exhibit significantly improved fracture toughness as compared to CE, CE/ZAA, EP/GA and EP/GA/ZAA. Although 60CE/40 EP/GA/ZAA and 50CE/50 EP/GA/ZAA display lower flexural strength than CE (or CE/ZAA) owing to the decreased rigid triazine ring networks, all CE/EP/GA/ZAA systems have higher flexural strength than EP/GA (or EP/GA/ZAA). 60CE/40 EP/GA/ZAA, 50CE/50 EP/GA/ZAA and 40CE/

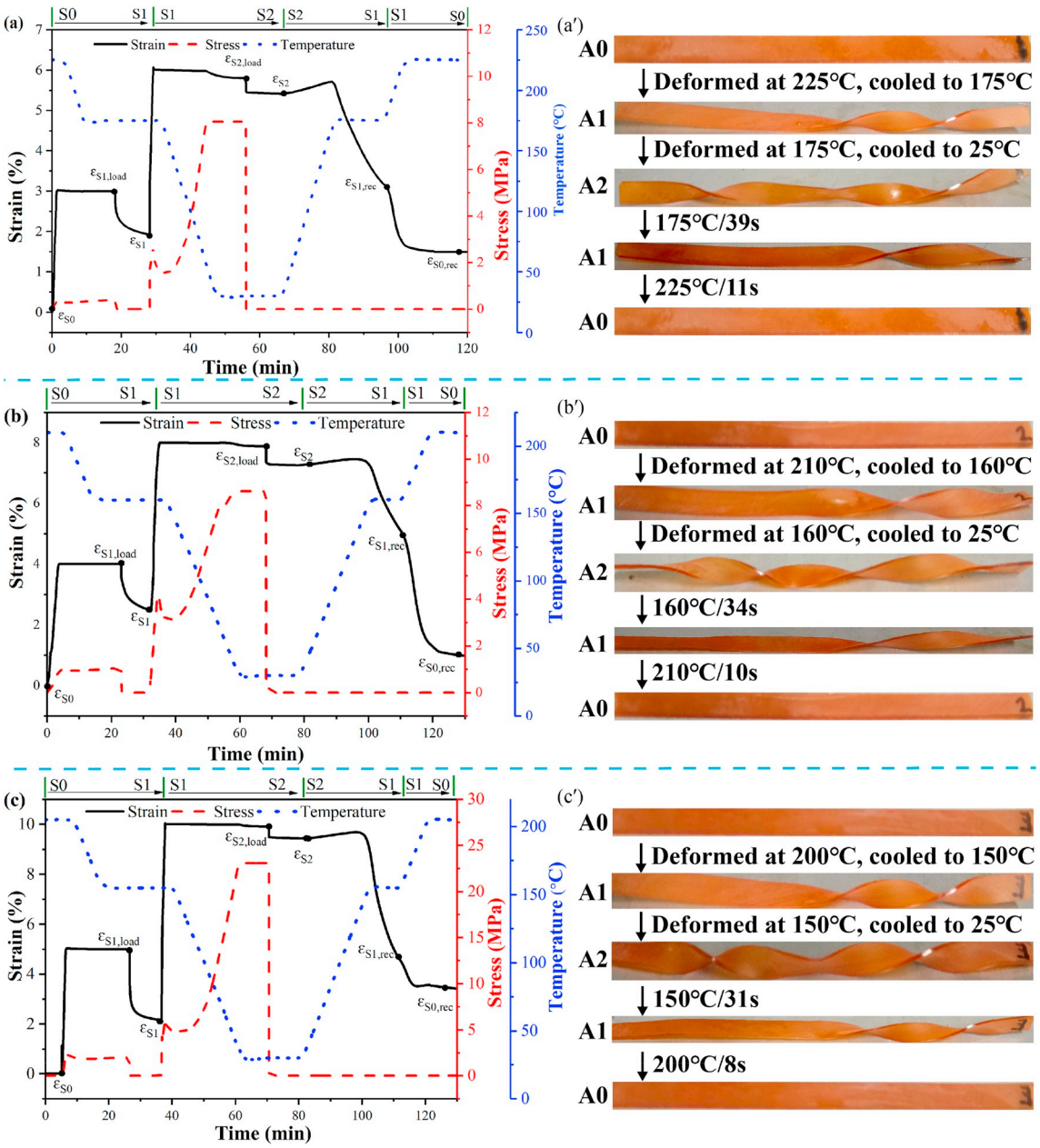

Fig. 7. Triple-shape memory effect and images demonstration of CE/EP/GA/ZAA: 60CE/40 EP/GA/ZAA (a, a′), 50CE/50 EP/GA/ZAA (b, b′), 40CE/60 EP/GA/ZAA (c, c′).

60 EP/GA/ZAA also display higher mechanical property than 90CE/10 EP/GA/ZAA and 10CE/90 EP/GA/ZAA systems, the main reason is the fact that EP nanostructures can effectively consume energy as indicated by the tortuous microcracks within matrix (Fig. 3 and Fig. S3). The SEM images of fracture surfaces of 60CE/40 EP/GA/ZAA, 50CE/50 EP/GA/ZAA, 40CE/60 EP/GA/ZAA and EP/GA/ZAA show rough fracture surfaces (Fig. 6b–6d and 6f), indicating that the resulting polymers exhibit certain degree of toughness. Moreover, it can be found that 60CE/40 EP/GA/ZAA, 50CE/50 EP/GA/ZAA, 40CE/60 EP/GA/ZAA show rougher fracture surfaces than CE, CE/ZAA, EP/GA, 90CE/10 EP/GA/ZAA and 10CE/90 EP/GA/ZAA, indicating that CE/EP/GA/ZAA systems can consume more energy and have better toughness.

Table 1
Triple-shape memory property obtained from Fig. 7a–7c.

Samples	R_f (%)		R_r (%)	
	S0→S1	S1→S2	S2→S1	S1→S0
60CE/40 EP/GA/ZAA	63	97	64	83
50CE/50 EP/GA/ZAA	62	94	47	88
40CE/60 EP/GA/ZAA	44	93	68	67

3.4. Triple-shape memory behavior

Because 60CE/40 EP/GA/ZAA, 50CE/50 EP/GA/ZAA, 40CE/60 EP/GA/ZAA show broad glass transition region (Fig. 5a), they may have good deformation ability [44,45]. The CE/EP/GA/ZAA systems show high tensile stain (~43%) at break at T_g + 35 °C (Fig. S5) and have excellent dual-shape memory behavior with a R_f of 83.3–91.0% and a R_r of 92.7–95.4% after 5 cycles (Fig. S6 and Table S1). The triple-shape memory effect of CE/EP/GA/ZAA systems were investigated in detail as shown in Fig. 7. Table 1 summarizes the R_f and R_r values of CE/EP/GA/ZAA systems. During the shape memory cycle processes of CE/EP/GA/ZAA systems (Fig. 7a–7c), the original rectangle samples are

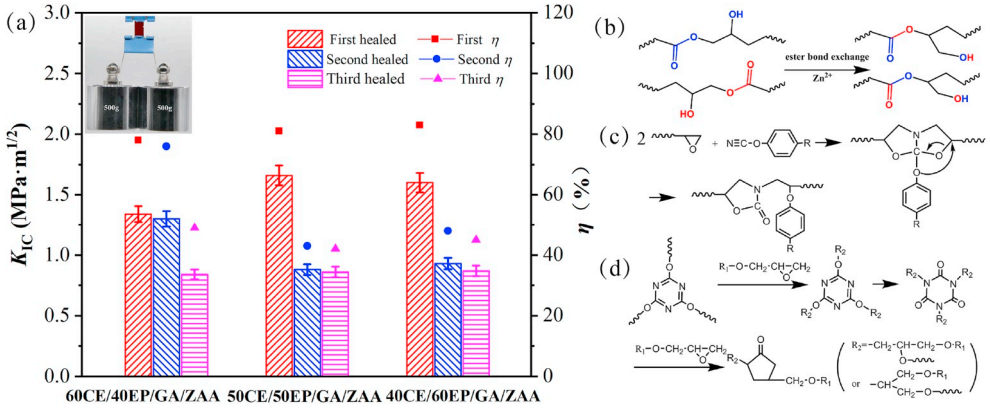

Fig. 8. Fracture toughness and self-healing efficiency of the healed CE/EP/GA/ZAA systems (a) and self-healing mechanism (b–d).

heated to 200–225 °C for 5 min first, and then stretched to 3–4% strain with the stretch rate of 2%/min, cooling to 150–175 °C, part of the chains become frozen and the first temporary shape S1 can be fixed, the obtained $R_{f,\ S0\rightarrow S1}$ is 44–63%. The chains can continue to move after an additional 4% strain is applied to the sample, the second temporary shape S2 can be fixed, and the $R_{f,\ S1\rightarrow S2}$ of 93–97% can be obtained after cooled to room temperature and reload the force. Reheating the samples with temporary shape S2 to 150–175 °C, their shape recovery can be activated to shape S1 and the $R_{r,\ S2\rightarrow S1}$ is 47–68%. When the temperature continues to rise to 200–225 °C, the recovered shape S1 can recover to the original shape S0 and the final shape recovery rate $R_{r,\ S1\rightarrow S0}$ is 67–83%.

Images demonstration of triple-shape memory effect of CE/EP/GA/ZAA systems is also shown in Fig. 7a′–7c′). One side of a longer strip samples (A0) are deformed to a spiral (A1) at higher temperature (200–225 °C), and then cooling to a lower temperature (150–175 °C) under load, another side of sample is deformed to an inverse spiral (A2), which can be fixed after cooled to 25 °C and unloading the external force. When the deformed samples are heated to 150–175 °C and then to 200–225 °C, their shapes (A2) can recover to the temporary shape (A1) and the original shape (A0), respectively.

3.5. Self-healing behavior

CE/EP/GA/ZAA systems contain dynamic ester linkages resulting from the reaction of EP and GA, and the reversible transesterification reaction can be happened between ester group and hydroxyl group in the presence of catalyst ZAA and new ester groups and hydroxyl groups are formed before a dynamic equilibrium of transesterification is re-established. Therefore, self-healing behavior may occur in CE/EP/GA/ZAA systems [32–34]. Fig. 8 shows the fracture toughness and the healing efficiency η of the healed CE/EP/GA/ZAA systems, and self-healing mechanism. After the first healing cycle at 200 °C for 2 h, the fractured 60CE/40 EP/GA/ZAA, 50CE/50 EP/GA/ZAA and 40CE/60 EP/GA/ZAA have the healing efficiencies of 78%, 81% and 83%, respectively (Fig. 8a). The healing efficiencies for 60CE/40 EP/GA/ZAA, 50CE/50 EP/GA/ZAA and 40CE/60 EP/GA/ZAA are 76%, 43% and 48%, respectively, after the second healing cycle at 200 °C for 2 h is completed. The third healing efficiencies can be close to 50% for CE/EP/GA/ZAA systems (Fig. 8a).

The ability of self-healing mainly results from the transesterification reaction in CE/EP/GA/ZAA systems as shown in Fig. 8b. When the fracture surfaces are tightly close together, the transesterification between β-hydroxyl groups and ester groups on the two crack surfaces might happen in the presence of the catalyst ZAA at 200 °C and form new ester groups and β-hydroxyl groups, thus chemical reaction can re-bond the two fracture surfaces together. In addition, CE/EP/GA/ZAA systems contain small amount of unreacted epoxy groups and –OCN groups that can react with each other (Fig. 8c), and the epoxy groups can react with the triazine ring in CE polymers at high temperature (Fig. 8d), which can aid in healing the crack surfaces. After the first healing cycle, the healing efficiencies significantly decrease owing to the reduced epoxy groups and –OCN groups in healed CE/EP/GA/ZAA systems. The second healed 50CE/50 EP/GA/ZAA sample can withstand 1000 g-weigh pull force, indicating the good healing ability. The fracture surfaces of samples can be bonded together and the cracks between the two fracture surfaces partially or completely disappear after treating at 200 °C for 2 h (Fig. S7a–7c). Some interfacial debonding regions can be observed from the fracture surface of the healed sample as marked by circles in Fig. S7d–7 g, which indicates the healing behavior.

4. Conclusions

In situ nanodomain structure in polymer networks with dynamic ester bonds were successfully constructed by catalyst-controlling the dynamic crosslinking behavior of compatible thermosetting CE/EP blend. The resulting CE/EP/GA/ZAA systems not only had adjustable T_g from 167 °C to 192 °C, but also exhibited high initial thermal decomposition temperatures of 337–353 °C. The existence of nanophase structure in polymer systems could increase the microcrack propagation path and effectively consume energy. CE/EP/GA/ZAA systems displayed excellent toughness of 1.7–2.0 MPa m$^{1/2}$ and high flexural strength of 87—135 MPa. Moreover, such thermosetting CE/EP/GA/ZAA systems could exhibit good triple-shape memory effect via thermal activation at 200–225 °C and 150–175 °C, respectively. The introduction of the dynamic ester bond as well as the residual epoxy group and –OCN groups could endow CE/EP/GA/ZAA with good self-healing ability, a healing efficiency of 78–83% could obtain for CE/EP/GA/ZAA systems. The healing efficiency could remain about 50% even after third healing cycle. The present strategy of in situ self-constructed nanodomain structure in thermosetting CE/EP/GA/ZAA offered a promising opportunity to improve the mechanical property and develop function materials.

Acknowledgement

The authors thank the National Natural Science Foundation of China (No. 51273135), and the support of the Priority Academic Program Development of Jiangsu Higher Education Institutions (PAPD), State and Local Joint Engineering Laboratory for Novel Functional Polymeric Materials.

Appendix A. Supplementary data

Supplementary data to this article can be found online at https://doi.org/10.1016/j.compositesb.2019.107438.

References

[1] Park HH, Sun K, Seong M, Kang M, Park S, Hong S, Jung H, Jang J, Kim J, Jeong HE. Lipid-hydrogel-nanostructure hybrids as robust biofilm-resistant polymeric materials. ACS Macro Lett 2018;8(1):64–9.

[2] Zhang Y, Zhang Z, Li J, Sui G. (3-aminopropyl) triethoxysilane grafted poly (dopamine)@Fe_3O_4 nanoparticles and their epoxy composites for functional application. Compos B Eng 2019;169:148–56.

[3] Rajaei M, Kim NK, Bickerton S, Bhattacharyya D. A comparative study on effects of natural and synthesised nano-clays on the fire and mechanical properties of epoxy composites. Compos B Eng 2019;165:65–74.

[4] Rafiee M, Nitzsche F, Laliberte J, Hind S, Robitaille F, Labrosse MR. Thermal properties of doubly reinforced fiberglass/epoxy composites with graphene nanoplatelets, graphene oxide and reduced-graphene oxide. Compos B Eng 2019; 164:1–9.

[5] Sandhya PK, Sreekal MS, Padmanabhan M, Jesitha K, Thomas S. Effect of starch reduced graphene oxide on thermal and mechanical properties of phenol formaldehyde resin nanocomposites. Compos B Eng 2019;167:83–92.

[6] Gong CK, Liang JJ, Hu W, Niu XF, Ma SW, Hahn HT, Pei QB. A healable, semitransparent silver nanowire-polymer composite conductor. Adv Mater 2013; 25(30):4186–91.

[7] Vijayan PP, Puglia D, Al-Maadeed, MAS A, Kenny JM, Thomas S. Elastomer/ thermoplastic modified epoxy nanocomposites: the hybrid effect of 'micro' and 'nano' scale. Math Sci Eng R 2017;116:1–29.

[8] Rosetti Y, Alcouffe P, Pascault JP, Gerard JF, Lortie F. Polyether sulfone-based epoxy toughening: from micro- to nano-phase separation via PES end-chain modification and process engineering. Materials 2018;11(10):1960–76.

[9] Poel GV, Goossens S, Goderis B, Groeninckx G. Reaction induced phase separation in semicrystalline thermoplastic/epoxy resin blends. Polymer 2005;46(24): 10758–71.

[10] Russell B, Chartoff R. The influence of cure conditions on the morphology and phase distribution in a rubber-modified epoxy resin using scanning electron microscopy and atomic force microscopy. Polymer 2005;46(3):785–98.

[11] Deeraj BDS, Saritha A, Joseph K. Electrospun styrene-butadiene copolymer fibers as potential reinforcement in epoxy composites: modeling of rheological and visco elastic data. Compos B Eng 2019;160:384–93.

[12] Yu RT, Zheng SX, Li XH, Wang J. Reaction-induced microphase separation in epoxy thermosets containing block copolymers composed of polystyrene and poly (ε-caprolactone): influence of copolymer architectures on formation of nanophases. Macromolecules 2012;45(22):9155–68.

[13] Cong H, Li L, Zheng S. Formation of nanostructures in thermosets containing block copolymers: from self-assembly to reaction-induced microphase separation mechanism. Polymer 2014;55(5):1190–201.

[14] Zhang CY, Li L, Zheng SX. Formation and confined crystallization of polyethylene nanophases in epoxy thermosets. Macromolecules 2013;46(7):2740–53.

[15] Lipic PM, Bates FS, Hillmyer MA. Nanostructured thermosets from self-assembled amphiphilic block copolymer/epoxy resin mixtures. J Am Chem Soc 1998;120: 8963–70.

[16] George SM, Puglia D, Kenny JM, Jyotishkumar P, Thomas S. Cure kinetics and thermal stability of micro and nanostructured thermosetting blends of epoxy resin and epoxidized styrene-block-butadiene-block-styrene triblock copolymer systems. Polym Eng Sci 2012;52(11):2336–47.

[17] Ritzenthaler S, Court F, David L, Girard-Reydet E, Leibler L, Pascault JP. ABC triblock copolymers/epoxy-diamine blends. 1. Keys to achieve nanostructured thermosets. Macromolecules 2002;35(16):6245–54.

[18] Fan WC, Wang L, Zheng SX. Nanostructures in thermosetting blends of epoxy resin with polydimethylsiloxane-block-poly(ε-caprolactone)-block-polystyrene ABC triblock copolymer. Macromolecules 2009;42:327–36.

[19] Guo QP, Thomann R, Gronski W, Staneva R, Ivanova R, Stuhn B. Nanostructures, semicrytalline morphology, and nanoscale confinement effect on the crystallization kinetics in self-organized block copolymer/thermoset blends. Macromolecules 2003;36(10):3635–45.

[20] Wu SY, Guo QP, Peng SH, Hameed N, Kraska M, Stühn B, Mai Y-W. Toughening epoxy thermosets with block ionomer complexes: a nanostructure-mechanical property correlation. Macromolecules 2012;45(9):3829–40.

[21] Wu SY, Guo QP, Kraska M, Stühn B, Mai Y-W. Toughening epoxy thermosets with block ionomers: the role of phase domain size. Macromolecules 2013;46(20): 8190–202.

[22] Gu AJ. High performance bismaleimide/cyanate ester hybrid polymer networks with excellent dielectric properties. Compos Sci Technol 2006;11–12:1749–55.

[23] Pellegrino M. Two-dimensional FTIR spectroscopy studies on the thermal-oxidative degradation of epoxy and epoxy-bis(maleimide) networks. Macromolecules 2003; 36(9). 3210–321.

[24] Li XD, Luo XY, Gu Y. A novel benzoxazine/cyanate ester blend with sea-island phase structures. Phys Chem Chem Phys 2015;17(29):19255–60.

[25] Amos Adeniyi, Oluranti Agboola, Rotimi Sadiku Emmanuel, Durowoju MO, Olubambi PA, Reddy AB, Ibrahim ID, Kupolati WK. Thermoplastic-thermoset nanostructured polymer blends. In: Thomas S, Shanks R, Chandrasekharakurup S, editors. Design and applications of nanostructured polymer blend and nanocomposite systems. William Andrew; 2016. p. 15–38.

[26] Garate H, Morales NJ, Goyanes S, D'Accorso NB. Miscibility, Phase separation, and mechanism of phase separation of epoxy/block-copolymer blends. In: Parameswaranpillai J, Hameed N, Pionteck J, Woo E, editors. Handbook of epoxy blends. Cham: Springer; 2015. p. 1–41.

[27] Wang Z, Li L, Fu YZ, Miao Y, Gu Y. Reaction-induced phase separation in benzoxazine/bismaleimide/imidazole blend: effects of different chemical structures on phase morphology. Mater Des 2016;107:230–7.

[28] Reghunadhan Nair CP, Mathew D, Ninan KN. Cyanate ester resins, recent developments. Adv Polym Sci 2001;155:47–68.

[29] Ding ZJ, Yuan L, Guan QB, Gu AJ, Liang GZ. A reconfiguring and self-healing thermoset epoxy/chain- extended bismaleimide resin system with thermally dynamic covalent bonds. Polymer 2018;147:170–82.

[30] Lu L, Fan J, Li G. Intrinsic healable and recyclable thermoset epoxy based on shape memory effect and transesterification reaction. Polymer 2016;105:10–8.

[31] Capelot M, Montarnal D, Tournilhac F, Leibler L. Metal-catalyzed transesterification for healing and assembling of thermosets. J Am Chem Soc 2012; 134(18):7664–7.

[32] Demongeot A, Mougnier SJ, Okada S, Soulie-Ziakovic C, Tournilhac F. Coordination and catalysis of Zn^{2+} in epoxy-based vitrimers. Polym Chem 2016;7 (27):4486–93.

[33] Lu L, Pan J, Li GQ. Recyclable high-performance epoxy based on transesterification reaction. J Mater Chem 2017;5(40):21505–13.

[34] Capelot M, Unterlass MM, Tournilhac F, Leibler L. Catalytic control of the vitrimer glass transition. ACS Macro Lett 2012;1(7):789–92.

[35] Ashcroft WR. Curing agents for epoxy resins. In: Ellis B, editor. Chemistry and technology of epoxy resins. Dordrecht: Springer; 1993. p. 37–71.

[36] Bowman CN, Kloxin CJ. Covalent adaptable networks: reversible bond structures incorporated in polymer networks. Angew Chem Int Ed 2012;51(18):4272–4.

[37] Roy N, Bruchmann B, Lehn JM. DYNAMERS: dynamic polymers as self-healing materials. Chem Soc Rev 2015;44(11):3786–807.

[38] Pernot H, Baumert M, Court F, Leibler L. Design and properties of co-continuous nanostructured polymers by reactive blending. Nat Mater 2002;1(1):54–8.

[39] Torbati AH, Nejad HB, Ponce M, Sutton JP, Mather PT. Properties of triple shape memory composites prepared via polymerization-induced phase separation. Soft Matter 2014;10(17):3112–21.

[40] –>Teng KC, Chang FC. Single-phase and multiple-phase thermoplastic thermoset polyblends .1. kinetics and mechanisms of phenoxy epoxy blends. Polymer 1993; 34(20):4291–9.

[41] Deng Y, Martin GC. Diffusion phenomena during cyanate resin cure. Polymer 1996; 37(16):3593–601.

[42] Deng Y, Martin GC. Effect of diffusional limitations on the gelation of cyanate ester resins. J Appl Polym Sci 1997;64(1):115–25.

[43] Fan J, Hu X, Yue CY. Static and dynamic mechanical properties of modified bismaleimide and cyanate ester interpenetrating polymer networks. J Appl Polym Sci 2003;88(8):2000–6.

[44] Xie T. Tunable polymer multi-shape memory effect. Nature 2010;464(7286): 267–70.

[45] Peterson GI, Childers EP, Li H, Dobrynin AV, Becker ML. Tunable shape memory polymers from α-amino acid-based poly(ester urea)s. Macromolecules 2017;50 (11):4300–8.